

A kilometer-scale asteroid inside Venus' orbit

B. T. Bolin^{1,2*}, W.-H. Ip³, F. J. Masci², Q. Ye⁴, E. A. Kramer⁵, G. Helou²,
 T. Ahumada⁴, M. W. Coughlin^{1,6}, M. J. Graham¹, R. Walters¹,
 K. P. Deshmukh⁷, C. Fremling¹, Z.-Y. Lin³, J. W. Milburn⁸, J. N. Purdum⁹,
 R. Quimby^{9,10}, D. Bodewits¹¹, C.-K. Chang¹², C.-C. Ngeow³, H. Tan³, C. Zhai⁵,
 P. van Dokkum¹³, M. Granvik^{14,15}, Y. Harikane^{16,17}, L. A. Mowla¹³, K. B. Burdge¹,
 E. C. Bellm¹⁸, K. De¹, S. B. Cenko^{19,20}, C. M. Copperwheat²¹, R. Dekany⁸,
 D. A. Duev¹, D. Hale⁸, M. M. Kasliwal¹, S. R. Kulkarni¹, T. Kupfer²²,
 A. Mahabal¹, P. J. Mróz¹, J. D. Neill¹, R. Riddle⁸, H. Rodriguez⁸, E. Serabyn⁵,
 R. M. Smith⁸, J. Sollerman²³, M. T. Soumagnac^{24,25}, J. Southworth²¹, L. Yan¹

¹Division of Physics, Mathematics and Astronomy, Caltech, Pasadena, CA 91125, USA, ²IPAC, Caltech, Pasadena, CA 91125, USA

³Institute of Astronomy, National Central University, Zhongli 32054, Taiwan. ⁴Department of Astronomy, University of Maryland, College Park, MD 20740, USA,

⁵Jet Propulsion Laboratory, Caltech, Pasadena, CA 91109, USA, ⁶School of Physics and Astronomy, University of Minnesota, Minneapolis, MN 55455, USA,

⁷Department of Engineering, Indian Institute of Technology, Bombay, Powai, India, ⁸Caltech Optical Observatory, Pasadena, CA 91125, USA,

⁹Department of Astronomy, San Diego State University, San Diego, CA 92182, USA, ¹⁰Kavli Institute for the Physics and Mathematics of the Universe, University of Tokyo, Tokyo, Japan,

¹¹Department of Physics, Leach Science Center, Auburn University, Auburn, AL 36849, USA,

¹²Institute of Astronomy and Astrophysics, Academia Sinica, P.O. Box 23-141, Taipei 10617, Taiwan ¹³Department of Astronomy, Yale University, New Haven, CT 06511, USA,

¹⁴Department of Physics, P.O. Box 65 00014, University of Helsinki, Finland ¹⁵Asteroid Engineering Lab, Onboard Space Systems, Luleå University of Technology, Kiruna, Sweden

¹⁶Department of Physics and Astronomy, University College of London, London WC1E 6BT, UK, ¹⁷National Astronomical Observatory of Japan, 2-21-1 Osawa, Mitaka, Tokyo 181-8588, Japan,

¹⁸Department of Astronomy, University of Washington, Seattle, WA 98195, USA, ¹⁹Division of Astrophysical Sciences, NASA Goddard Space Flight Center, Greenbelt, MD 20771, USA,

²⁰Joint Space Science Institute, University of Maryland, College Park, MD 20740, USA, ²¹Astrophysical Research Institute, Liverpool John Moores University, Liverpool L2 2QP, UK,

²²Department of Physics and Astronomy, Texas Tech University, Box 1051, Lubbock, TX 79409, USA,

²³Department of Astronomy, The Oskar Klein Centre, Stockholm University, SE-106 91 Stockholm, Sweden

²⁴Lawrence Berkeley National Laboratory, University of California, Berkeley, CA 94720, USA,

²⁵Department of Particle Physics and Astrophysics, Weizmann Institute of Science, Rehovot 7610001, Israel

*To whom correspondence should be addressed; bbolin@caltech.edu

Abstract

Near-Earth asteroid models predict the existence of bodies located inside the orbit of Venus. Despite searches up to the end of 2019, none had been found. Here we report the discovery by the Zwicky Transient Facility of the first known inner-Venus asteroid, (594913) 'Ayló'chaxnim, possessing an aphelion distance of 0.65 au and is \sim 2 km in size. While it is possible that 'Ayló'chaxnim is the largest of its kind, we find that its discovery is surprising in the context of population models which predict an expected observed count close to zero. If this discovery is not a statistical fluke, 'Ayló'chaxnim may be a representative example of a larger population of asteroids located inside the orbit of Venus than is described in contemporary asteroid models.

Main Text

Almost all 1 million known asteroids are exterior to the Earth's orbit whereas only a fraction of a percent are located entirely inside its orbit (1, 2). Despite the proposal of searches with ground-based telescopes (3, 4) and the formulation of dynamical models predicting that a small fraction of the near-Earth asteroid population (5, 6) should be located entirely within the orbit of Venus, none have yet been directly observed. Here we report the first discovery of an asteroid with an orbit entirely interior to the orbit of Venus, 'Ayló'chaxnim (7), that was first detected by the Palomar Observatory Zwicky Transient Facility (ZTF) on the Samuel Oschin Telescope (8, 9) on 2020 January 4 in four separate 30 s *r*-band exposures and moving \sim 130 arcseconds per hour (Fig. 1A-B). Postulated asteroids internal to the orbit of Venus have been provisionally referred to as "Vatiras" in the literature, a modification of the Atira name for asteroids interior to the orbit of the Earth (10).

The initial detection of (594913) 'Ayló'chaxnim was made in the evening twilight sky while it was \sim 40 degrees from the Sun in what we call the “Twilight Survey” [(4), (Fig. 2A)] which took place between 2019 September 20 and 2020 January 30. The ZTF Twilight Survey scheduler (11) uses a nearly contiguous 10 field pattern providing \sim 470 square degrees of sky coverage per Twilight Survey session in sky that has elevation as small as \sim 20 degrees and airmass as large as \sim 3.0. Each Twilight Survey session lasts 20-25 minutes where each field is imaged four times with 30 s exposures in *r* band, resulting in a \sim 5 minute spacing between exposures in each of the 10 fields. This allows for the positive identification of objects moving as slow as \sim 8 arcseconds per hour to as fast as >1500 arcseconds per hour by the ZTF processing system (12, 13). The sensitivity in each of the 30 s *r*-band exposures is degraded due to the extinction caused by the higher airmass of the observations and the higher sky background resulting in a limiting magnitude being closer to $V \sim 20$ [(4), Fig. S5D] compared to the nominal ZTF limiting magnitude of $V \sim 21$ (8, 9).

The strategy of the Twilight Survey is based on an initial version of the survey that ran in late 2018 and the first half of 2019 (4, 14). The current Twilight Survey is executed on each night, weather-permitting, alternating between evening and morning twilight. In total, the Twilight Survey was carried out 90 times between 2019 September 20 and 2020 January 30 split into 47 mornings and 43 evenings. The complete Sun-centered sky coverage of these 100 observing sessions is presented in Fig. 2. In total, \sim 50,000 square degrees of the sky was covered four times during the entirety of the Twilight Survey discussed in this analysis. The current Twilight Survey is ongoing, but poor weather in 2020 February and March limits this analysis to survey dates between 2019 September 20 and 2020 January 30.

The use of the ZTF telescope at low telescope altitudes during astronomical twilight time enables observations at Solar elongations 35-60 degrees from the Sun (Fig. 2B). Nearly half of the sky covered by the Twilight Survey is within the maximum Solar elongation distance

of inner-Venus objects (IVOs) of $\arcsin(0.72 \text{ au} / 1.0 \text{ au}) \simeq 46$ degrees (Fig. 2B) where the perihelion distance of Venus is ~ 0.72 au. Theoretical asteroid models describe the majority of IVOs, up to $\sim 80\%$ of their population, as having maximum possible Solar elongation angles that are reachable by the Twilight survey (6) making it the ideal survey for detecting a population of IVOs (Fig. 2C). The ZTF Twilight survey covers more sky at small Solar elongations inhabited by IVOs compared to other major asteroid surveys, [(14), Fig. 1], giving ZTF an advantage in detecting asteroids inside the orbit of Venus.

Additional data obtained with the Spectral Energy Distribution Machine (SEDM) on the Palomar 60-inch telescope (15) on 2020 January 8 and the Kitt Peak Electron Multiplying CCD Demonstrator (KPED) mounted on the Kitt Peak 84-inch telescope (16) on 2020 January 9 indicated this asteroid as having a likely aphelion distance of ~ 0.65 au. Follow-up data obtained by our team and other observers during 2020 January 4-23 more precisely confirmed its aphelion distance of 0.653817 ± 0.000825 , well within the 0.72 au perihelion distance of Venus, confirming the discovery of the first inner-Venus asteroid (Fig. 3). During its next apparition in 2020, the orbit of 'Ayló'chaxnim was further refined by our team on 2020 November 24-26 using SEDM (Fig. 1C) and Lulin Optical Telescope extending its orbital arc to 327 days drastically improving the precision of 'Ayló'chaxnim's orbital elements to one part in a million [(4), Tab. S1].

As noted by (17) and (18), one of the main features of the long term orbital evolution of 'Ayló'chaxnim is its capture into mean motion resonances with Venus such as the 3:2 mean motion resonance located at 0.552 au. From our orbital solution of 'Ayló'chaxnim which was dramatically improved with follow-up observations taken in 2020 November, we confirm that the nominal orbit of 'Ayló'chaxnim enters the 3:2 mean motion with Venus after ~ 0.06 Myrs [(4), Fig. S3A]. The amplitude of libration is initially large but dramatically shrinks after close encounters with Mercury ~ 0.01 Myrs later. The result of 'Ayló'chaxnim being in resonance

with Venus is that it increases the minimum approach distance to Venus protecting it from close encounters with the planet similar to the effect of the 2:3 mean motion resonances between Neptune and Pluto protecting the latter from encounters with the former (19). The asteroid 'Ayló'chaxnim will remain in resonance with Venus for ~ 0.01 Myrs when it begins jumping in and out of the 3:2 mean motion resonance for the next ~ 0.1 Myrs.

Further integration of the orbit of 'Ayló'chaxnim reveals that it has only recently been located within the orbit of Venus having an aphelion distance smaller than the perihelion distance of Venus of 0.718 au in the last ~ 1 Myrs, and will remain inside the orbit of Venus for another ~ 1.5 Myrs as seen for the evolution of one possible example 'Ayló'chaxnim orbit [(4), Fig. S3B]. It is noteworthy that the close perihelion of 'Ayló'chaxnim with the orbit of Mercury is similar to how many ecliptic comets have a close perihelion with the orbit of Jupiter indicating the evolution of their orbit from close planetary encounters (20). On average, the orbital clones of 'Ayló'chaxnim spend ~ 2 Myrs of the first ~ 4 Myrs of their orbital lifetime with aphelia within the orbit of Venus. This is in contrast with the previous work of (17) and (18) which found a much shorter residence time of <1 Myrs time that 'Ayló'chaxnim remained inside the orbit of Venus integrated over the first ~ 4 Myrs using a less precise orbit of 'Ayló'chaxnim computed from observations spanning only a few days to weeks.

While the current precision of 'Ayló'chaxnim's orbit prevents predicting its orbital behavior on timescales exceeding a few 10 Myrs, it is apparent from its orbital evolution that it is a transitory inhabitant of the inner Venus region of the Solar System. The majority of orbital clones have several lunar distances encounters with Mercury, Venus and the Earth within 10-20 Myr that have the effect of exciting their orbits onto trajectories taking them on very close perihelion passages with the Sun as seen for one of the longer-lived orbital clones [(4), Fig. S3C]. The median time between the start time of the integration of the 'Ayló'chaxnim clones and their collision with a planet or the Sun is ~ 10 Myrs, and $\sim 90\%$ of the clones have collided with the

Sun or a planet by the 30 Myrs end time of the integration. The $\sim 10\%$ of clones that survived the first 30 Myrs were integrated further for a total of 50 Myrs total integration. In total, $\sim 13\%$ of the 'Ayló'chaxnim clones collided with the Sun, having a perihelion distance <0.005 au, $\sim 13\%$ collided with Mercury, $\sim 52\%$ collided with Venus, $\sim 16\%$ collided with the Earth and $\sim 2\%$ collided with Mars. The remaining 4% still survived by the end of the extended 50 Myr integration or were ejected from the Solar System. Previous works investigating inner-Venus objects describe a median collisional lifetime for inner-Venus objects of ~ 21 Myrs (10), a factor of 2 larger than the median lifetime of our 'Ayló'chaxnim clones. However, the proportion of 'Ayló'chaxnim clones colliding with the Sun, Mercury, Venus, Earth and Mars is similar to that of the general inner-Venus object population with the majority of the collisions happening with Venus.

Spectroscopic observations of 'Ayló'chaxnim made using the Keck telescope on 2020 January 23 indicate a reddish surface corresponding to colors of $g-r = 0.65 \pm 0.02$ mag, $r-i = 0.23 \pm 0.01$ mag and an absorption band at ~ 900 nm corresponding to $i-z = 0.11 \pm 0.02$ mag [(4), Fig. S1]. These data favor a silicate S-type asteroid-like composition (21) consistent with an origin from the inner Main Belt where S-type asteroids are the most plentiful (22), and in agreement with the expectations of near-Earth asteroid (NEA) models that predict asteroids with the orbital elements of 'Ayló'chaxnim [(4), Tab. S1, Fig. S2] should originate from the inner Main Belt (6). Independent spectroscopic observations obtained at around the same time also indicate S-type taxonomy (23).

The spectral and dynamical classification of 'Ayló'chaxnim can be examined one step further by comparing its source region probability with the NEA albedo model of (24) to estimate its albedo. Comparing our source region probabilities with the location of 'Ayló'chaxnim in the medium-resolution NEA albedo model, it is likely that 'Ayló'chaxnim has an albedo of ~ 0.2 , consistent with the typical albedo for S-type asteroids (25). It is unsurprising in the context of

the NEA albedo model that given its S-type-like spectrum 'Ayló'chaxnim would have a higher albedo since the NEA albedo model predicts that $\sim 60\%$ of inner-Venus objects with $15 < H < 18$ should have albedos exceeding 0.2 [(4), Fig. S4]. Combining our albedo estimate from the NEA albedo model of 0.2 with the estimate of the absolute magnitude and absolute magnitude uncertainty of $H = 16.4 \pm 0.8$ magnitudes for 'Ayló'chaxnim in the JPL Small-Body Database Browser, we measure a diameter of $\sim 1.6 \pm 0.6$ km making it one of the rare km-scale asteroids remaining to be discovered in the asteroid population described by contemporary NEA models (6). The number of IVOs within a 68.2% confidence interval encompassing 'Ayló'chaxnim's absolute magnitude in the NEA model is 0.3 ± 0.6 with the main source of uncertainty being from the estimate on 'Ayló'chaxnim's size.

We estimated the number of IVOs expected to have been discovered by ZTF by simulating ZTF observations of synthetic IVOs generated by the NEA population model (6) in comparison with our discovery of 'Ayló'chaxnim. We generated a synthetic IVO population from the NEA model (6) using a medium resolution version of the model with semi-major axis resolution element, $da = 0.05$ au, eccentricity resolution element $de = 0.02$, inclination resolution element $di = 2.0^\circ$ and absolute magnitude resolution element $dH = 0.25$ oversampling by a factor of 1,000 producing $\sim 3.0 \times 10^3$ inner-Venus objects with $15 < H < 18$. The a , e , i and H distributions of our synthetically generated IVOs from the NEA population models are plotted in Fig. 4 (A-D). To simulate the discovery and observations of our synthetic inner-Venus asteroids by ZTF, we used the complete list of ZTF telescope pointings taken during the Twilight Survey between 2019 September 20 UTC and 2020 January 30 UTC (Fig. 2) with a survey simulator taking into account the apparent brightness of the synthetic IVOs in the survey simulation [(4), Fig. S5C]. The output of the survey simulator produces synthetic inner-Venus asteroids detections that can be used to roughly estimate the completeness of the ZTF survey in detecting inner-Venus asteroids. The IVO detection completeness in the Twilight survey is $18 \pm 2\%$ (Fig. 4A-D),

therefore, we expect 0.05 ± 0.09 IVOs to have been discovered during our observations. We also note that the completeness of detecting IVOs drops drastically with smaller values of Q than the $Q \sim 0.65$ au of 'Ayló'chaxnim as seen in Fig. 2C suggesting that its detection was just within the limits of the Twilight survey.

While ZTF's detection efficiency is still appreciable, our discovery of one inner-Venus asteroid would have been unlikely according to the current NEA model (6). If not a fluke, a possible explanation for the discovery of 'Ayló'chaxnim despite its low chance of discovery is that it could have originated from a larger population of asteroids inside the orbit Venus than described in contemporary asteroid models. A potential explanation for a larger population of asteroids inside the orbit of Venus could be an additional source of asteroids located in stability regions closer to the Sun such as those located inside the orbit of Mercury at ~ 0.1 - 0.2 (26), where km-scale asteroids could have previously gone undetected (27), and can remain stable and intact over the age of the Solar System (28–30).

References and Notes

1. R. P. Binzel, V. Reddy, T. L. Dunn, “The Near-Earth Object Population: Connections to Comets, Main-Belt Asteroids, and Meteorites”. In *Asteroids IV*, Michel, Patrick and DeMeo, Francesca E. and Bottke, William F., Eds. (University of Arizona Press, Tucson, 2015), pp. 243–256.
2. R. Jedicke, *et al.*, *Asteroids IV* pp. 795–813 (2015).
3. G. Masi, *Icarus* **163**, 389 (2003).
4. Materials and methods are available as supplementary materials.
5. W. F. Bottke, *et al.*, *Icarus* **156**, 399 (2002).
6. M. Granvik, *et al.*, *Icarus* **312**, 181 (2018).
7. B. T. Bolin, *et al.*, *Minor Planet Electronic Circulars* **2020-A99** (2020).
8. E. C. Bellm, *et al.*, *Publications of the Astronomical Society of the Pacific* **131**, 018002 (2019).
9. M. J. Graham, *et al.*, *Publications of the Astronomical Society of the Pacific* **131**, 078001 (2019).
10. S. Greenstreet, H. Ngo, B. Gladman, *Icarus* **217**, 355 (2012).
11. E. C. Bellm, *et al.*, *Publications of the Astronomical Society of the Pacific* **131**, 068003 (2019).
12. F. J. Masci, *et al.*, *Publications of the Astronomical Society of the Pacific* **131**, 018003 (2019).

13. D. A. Duev, *et al.*, *Monthly Notices of the Royal Astronomical Society* **486**, 4158 (2019).
14. Q. Ye, *et al.*, *Astronomical Journal* **159**, 70 (2020).
15. N. Blagorodnova, *et al.*, *Publications of the Astronomical Society of the Pacific* **130**, 035003 (2018).
16. M. W. Coughlin, *et al.*, *Monthly Notices of the Royal Astronomical Society* **485**, 1412 (2019).
17. S. Greenstreet, *Monthly Notices of the Royal Astronomical Society* **493**, L129 (2020).
18. C. de la Fuente Marcos, R. de la Fuente Marcos, *Monthly Notices of the Royal Astronomical Society* **494**, L6 (2020).
19. D. Nesvorný, F. Roig, S. Ferraz-Mello, *Astronomical Journal* **119**, 953 (2000).
20. M. Duncan, H. Levison, L. Dones, “Dynamical evolution of ecliptic comets”. In *Comets II*, Festou, Michel C. and Keller, H. Uwe and Weaver, Harold A., Eds. (University of Arizona Press, Tucson, 2004), pp. 193–204.
21. S. J. Bus, R. P. Binzel, *Icarus* **158**, 146 (2002).
22. F. E. DeMeo, B. Carry, *Nature* **505**, 629 (2014).
23. M. Popescu, *et al.*, *Monthly Notices of the Royal Astronomical Society* **496**, 3572 (2020).
24. A. Morbidelli, *et al.*, *Icarus* **340**, 113631 (2020).
25. F. E. DeMeo, B. Carry, *Icarus* **226**, 723 (2013).
26. N. W. Evans, S. Tabachnik, *Nature* **399**, 41 (1999).

27. A. J. Steffl, N. J. Cunningham, A. B. Shinn, D. D. Durda, S. A. Stern, *Icarus* **223**, 48 (2013).
28. D. Vokrouhlický, P. Farinella, W. F. Bottke, *Icarus* **148**, 147 (2000).
29. W. F. Bottke, *et al.*, *Icarus* **179**, 63 (2005).
30. A. Shannon, A. P. Jackson, D. Veras, M. Wyatt, *Monthly Notices of the Royal Astronomical Society* **446**, 2059 (2015).
31. S. Keys, *et al.*, *Publications of the Astronomical Society of the Pacific* **131**, 064501 (2019).
32. D. J. Tholen, R. J. Whiteley, *AAS/Division for Planetary Sciences Meeting Abstracts* #30 (1998), vol. 30 of *AAS/Division for Planetary Sciences Meeting Abstracts*, p. 16.04.
33. O. Vaduvescu, *et al.*, *Astronomy & Astrophysics* **609**, A105 (2018).
34. R. Dekany, *et al.*, *Publications of the Astronomical Society of the Pacific* **132**, 038001 (2020).
35. Q. Ye, *et al.*, *Publications of the Astronomical Society of the Pacific* **131** (2019).
36. M. Rigault, *et al.*, *Astronomy & Astrophysics* **627**, A115 (2019).
37. J. B. Oke, *et al.*, *Publications of the Astronomical Society of the Pacific* **107**, 375 (1995).
38. J. K. McCarthy, *et al.*, *Blue channel of the Keck low-resolution imaging spectrometer* (1998), vol. 3355 of *Society of Photo-Optical Instrumentation Engineers (SPIE) Conference Series*, pp. 81–92.
39. D. Kinoshita, *et al.*, *Chinese Journal of Astronomy and Astrophysics* **5**, 315 (2005).
40. D. A. Perley, *Publications of the Astronomical Society of the Pacific* **131**, 084503 (2019).

41. Gaia Collaboration, *et al.*, *Astronomy & Astrophysics* **595**, A1 (2016).
42. Gaia Collaboration, *et al.*, *Astronomy & Astrophysics* **616**, A1 (2018).
43. H. Raab, Astrometrica: Astrometric data reduction of CCD images, *Astrophysics Source Code Library*, record:1203.012. <http://www.astrometrica.at>. Accessed: 2021 August 26.
44. J. L. Tonry, *et al.*, *Astrophysical Journal Supplement* **750**, 99 (2012).
45. H. Rein, S.-F. Liu, *Astronomy & Astrophysics* **537**, A128 (2012).
46. H. Rein, D. S. Spiegel, *Monthly Notices of the Royal Astronomical Society* **446**, 1424 (2015).
47. W. F. Bottke, *et al.*, *Icarus* **156**, 399 (2002).
48. W. F. Bottke, Jr., D. Vokrouhlický, D. P. Rubincam, D. Nesvorný, *Annual Review of Earth and Planetary Sciences* **34**, 157 (2006).
49. M. Granvik, *et al.*, *Astronomy & Astrophysics* **598**, A52 (2017).
50. B. T. Bolin, M. Delbo, A. Morbidelli, K. J. Walsh, *Icarus* **282**, 290 (2017).
51. A. Morbidelli, R. Gonczi, C. Froeschle, P. Farinella, *Astronomy & Astrophysics* **282**, 955 (1994).
52. A. Milani, G. F. Gronchi, *Theory of Orbital Determination* (Cambridge University Press, 2010).
53. J. Wisdom, *Icarus* **56**, 51 (1983).
54. P. Vereš, *et al.*, *Icarus* **261**, 34 (2015).

55. R. Jedicke, B. Bolin, M. Granvik, E. Beshore, *Icarus* **266**, 173 (2016).
56. C. A. Thomas, *et al.*, *Astronomical Journal* **142**, 85 (2011).
57. D. A. Oszkiewicz, *et al.*, *Icarus* **219**, 283 (2012).
58. P. Pravec, A. W. Harris, P. Kušnírák, A. Galád, K. Hornoch, *Icarus* **221**, 365 (2012).
59. B. D. Warner, A. W. Harris, P. Pravec, *Icarus* **202**, 134 (2009).
60. S. P. Naidu, S. R. Chesley, D. Farnocchia, Near-Earth Object Survey Simulation Software, <https://github.com/AsteroidSurveySimulator/objectsInField>. Accessed: 2021 August 26.
61. F. E. DeMeo, R. P. Binzel, S. M. Slivan, S. J. Bus, *Icarus* **202**, 160 (2009).

Acknowledgements

Acknowledgements

Based on observations obtained with the Samuel Oschin Telescope 48-inch and the 60-inch Telescope at the Palomar Observatory as part of the Zwicky Transient Facility project. ZTF is supported by a collaboration including Caltech, IPAC, the Weizmann Institute for Science, the Oskar Klein Center at Stockholm University, the University of Maryland, the University of Washington, Deutsches Elektronen-Synchrotron and Humboldt University, Los Alamos National Laboratories, the TANGO Consortium of Taiwan, the University of Wisconsin at Milwaukee, and Lawrence Berkeley National Laboratories. Operations are conducted by COO, IPAC, and UW.

The KPED team thanks the National Science Foundation and the National Optical Astronomical Observatory for making the Kitt Peak 2.1-m telescope available. We thank the observatory

staff at Kitt Peak for their efforts to assist KPED operations. The KPED team thanks the National Science Foundation, the National Optical Astronomical Observatory, the Caltech Space Innovation Council and the Murty family for support in the building and operation of KPED. In addition, they thank the CHIMERA project for use of the Electron Multiplying CCD (EMCCD). The authors would like to thank Alessandro Morbidelli for useful discussion in the interpretation of the first inner-Venus asteroid discovery as well as providing the synthetic asteroid population used to model our survey efficiencies. The authors would also like to thank Thomas A. Prince for helpful discussion involving the Twilight survey observations and helping with communications involving the naming of 'Ayló'chaxnim.

Some of the data presented herein were obtained at the W. M. Keck Observatory, which is operated as a scientific partnership among the California Institute of Technology, the University of California and the National Aeronautics and Space Administration. The Observatory was made possible by the generous financial support of the W. M. Keck Foundation.

The authors wish to recognize and acknowledge the very significant cultural role and reverence that the summit of Maunakea has always had within the indigenous Hawaiian community. We are most fortunate to have the opportunity to conduct observations from this mountain.

This work has made use of data from the European Space Agency (ESA) mission *Gaia* (<https://www.cosmos.esa.int/gaia>), processed by the *Gaia* Data Processing and Analysis Consortium (DPAC, <https://www.cosmos.esa.int/web/gaia/dpac/consortium>). Funding for the DPAC has been provided by national institutions, in particular the institutions participating in the *Gaia* Multilateral Agreement.

Part of this work was carried out at the Jet Propulsion Laboratory, California Institute of Technology, under contract with NASA.

Funding

ZTF is supported by the National Science Foundation under Grant No. AST-1440341.

SED Machine is based upon work supported by the National Science Foundation under Grant No. 1106171

M.W.C. acknowledges support from the National Science Foundation with grant number PHY-2010970.

C.F. gratefully acknowledges the support of his research by the Heising-Simons Foundation (#2018-0907).

B.T.B., G.H., F.J.M. and E.K. acknowledge support from NASA with grant number 80NSSC19K0780.

Authors Contributions

B.T.B. discovered 'Ayló'chaxnim with the ZTF Twilight survey and realized it had an orbit inferior to Venus', led the study, led the writing of the manuscript, reviewed and scanned all candidate asteroid detections for the duration of this study, helped design and secure time for the Twilight survey and for follow-up, prepared and executed follow-up observations, reduced the photometric and spectroscopic data, did the astrometry, orbit determination, helped generate the synthetic NEA population, calculated the survey completeness and estimates of the inner-Venus asteroid population. W.-H.I. helped initiate, design and secure P48 time for the ZTF Twilight. F.J.M. served as the Science Data System Lead of the ZTF collaboration, wrote and maintained software for extraction of moving objects in ZTF data, calculated the survey completeness, maintained the ZTF data system, helped secure P48 time for the ZTF Twilight survey, helped design and initiate the Twilight survey. Q.Y. contributed code used to schedule the ZTF survey and contributed improvements to the moving object identification pipeline, and helped initiate

and design the Twilight survey. E.A.K. monitored the NEA discovery performance of the ZTF survey. G.H. helped with the interpretation of the completeness calculation, helped prepare the manuscript, served as the Primary Investigator of the team observing NEAs with ZTF and as the Data Archive Director of the ZTF collaboration, helped design the cadence, secure P48 time for the ZTF Twilight survey, is one of its initiators and helped name 'Ayló'chaxnim. T.A. and M.W.C. performed follow-up observations of 'Ayló'chaxnim with KPED and contributed to the reduction of photometry. M.J.G. served as the Project Scientist of ZTF, secured time with Keck I and took spectroscopic observations of 'Ayló'chaxnim with Keck I/LRIS and reduced spectral data. R.W. performed follow-up observations of 'Ayló'chaxnim with SEDM. K.P.D. contributed to planning follow-up observations of 'Ayló'chaxnim. C.F. contributed to the planning of spectroscopy observations of 'Ayló'chaxnim with Keck and spectroscopic data reduction. Z.-Y.L. contributed to the interpretation of the 'Ayló'chaxnim spectroscopy data. J.W.M. contributed to follow-up observations of 'Ayló'chaxnim. J.N.P. and R.Q. contributed to the reduction of photometry and follow-up observations of 'Ayló'chaxnim. D.B. contributed to the interpretation of minor body observations by the P48. C.-K.C., C.-C.N. and H.T. contributed to securing time with the P48 for ZTF Solar System observations. C.Z., C.M.C and J.S. were members of the team that conducts follow-up observations of ZTF Solar System discoveries. P.D. and L.A.M. helped secure time for follow-up observations of 'Ayló'chaxnim. M.G. helped generate the synthetic NEA population. Y.H. helped secure Keck time for follow-up of 'Ayló'chaxnim. K.B.B. and K.D. contributed to the reduction of Keck/LRIS spectroscopy data of 'Ayló'chaxnim. E.C.B. served as the Survey Scientist of the ZTF collaboration and scheduled the observations taken with the P48 during the ZTF Twilight survey. S.B.C. contributed to the planning of P48 time used in the Twilight survey. D.A.D, A.M. and P.J.M. wrote and maintained software and machine learning algorithms for the ZTF data pipeline and identification of sources in ZTF data. In addition, A.M. served as the Machine Learning Lead for the ZTF collaboration. R.D. served as

the Project Manager of the ZTF collaboration and contributed to the design and construction of the ZTF camera. D.H. contributed to the design and construction of the ZTF camera. M.M.K. served as the Primary Investigator of the Global Relay of Observatories Watching Transients Happen (GROWTH) team for follow-up of ZTF discoveries. S.R.K. served as the Principal Investigator of the ZTF collaboration and survey. T.K. and M.T.S. contributed to the ZTF calibration pipeline. J.D.N. contributed to SEDM operations and observations of 'Ayló'chaxnim. R.R. contributed to maintaining ZTF operations. H.R. contributed to SEDM operations. E.S. contributed to KPED operations and observations of 'Ayló'chaxnim. R.M.S. served as the Lead Camera Engineer for the ZTF survey and lead the design and construction of the ZTF camera. J.S. contributed to SEDM operations and observations of 'Ayló'chaxnim. L.Y. contributed to planning and securing of telescope time for follow-up observations of 'Ayló'chaxnim.

Data and materials availability

The software and data used for this work are available at

<https://dataVERSE.harvard.edu/dataVERSE/InnerVenusAsteroid> (doi:10.7910/DVN/UTAV4I Harvard DataVERSE). The orbit determination software FIND_ORB, REBOUND N-body orbit integration software (45) and the NEAR-EARTH OBJECT SURVEY SIMULATION software (60) are publicly available.

List of Supplementary Materials

Methods

Discovery, follow-up and orbital determination

Twilight Survey strategy

Discovery, follow-up and characterization observations

Visual imaging/spectroscopy reduction and astrometry

Dynamical evolution

Comparison with the NEA population

Estimating the ZTF inner-Venus asteroid population completeness

Figs. S1-S5

Tab. 1

References (31-55)

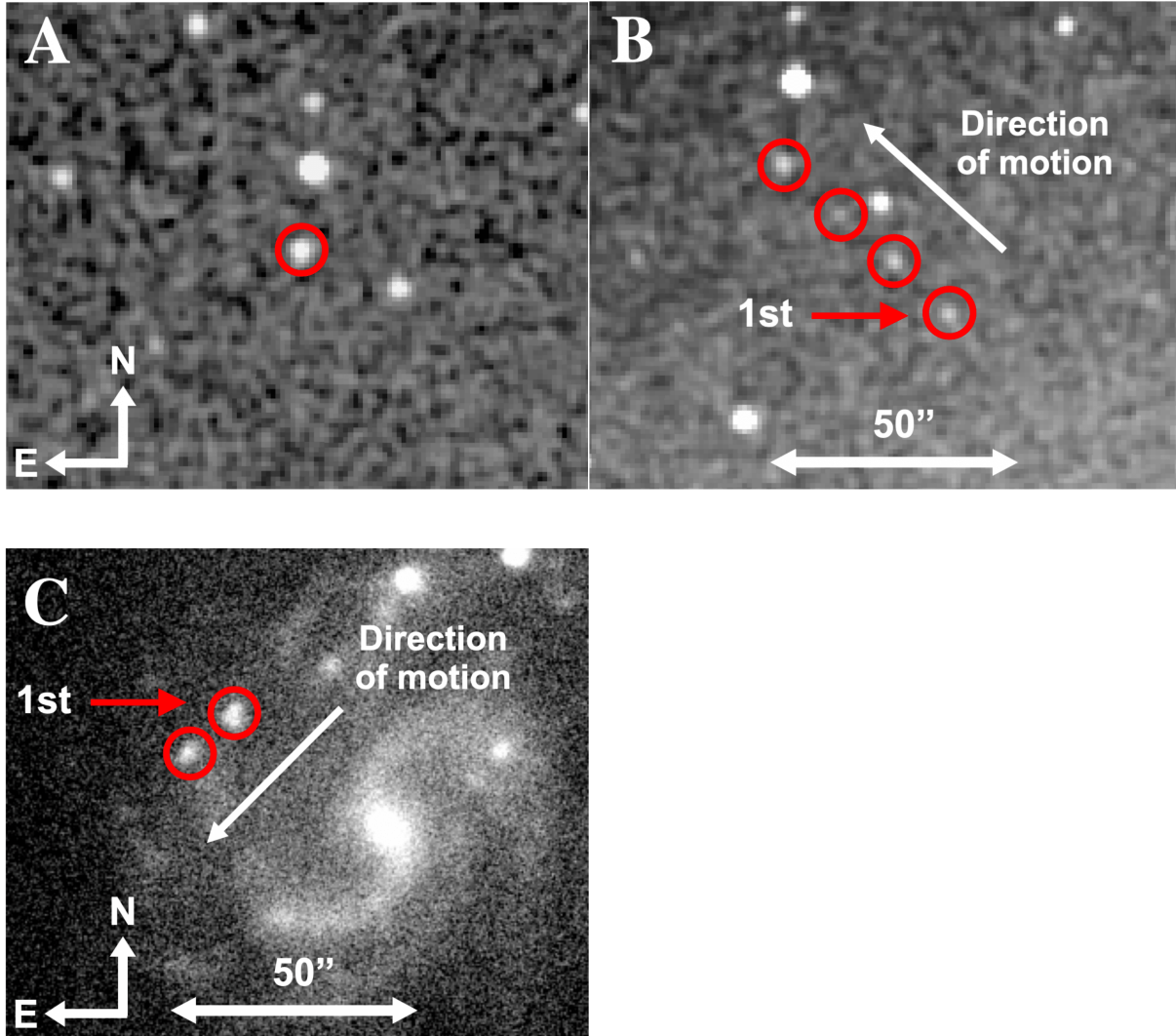


Figure 1: ZTF discovery and SEDM recovery images of 'Ayló'chaxnim. (A) Discovery 30 s r-band image of 'Ayló'chaxnim taken on 2020 January 4 UTC where 'Ayló'chaxnim is the detection located in the circle. (B) Composite image containing the four discovery 30 s r-band exposures covering 'Ayló'chaxnim made by stack on the rest frame of the background stars over a 22 minute time interval. The first detection has been labeled. The apparent faintness of the third detection is due to variations in transparency over the course of the 22 minute sequence that these images were taken. The asteroid was moving \sim 130 arcseconds per hour in the northeast direction while these images were being taken resulting in a \sim 10 arcseconds spacing between the detections of 'Ayló'chaxnim. (C) Composite image containing the two recovery 120 s r-band exposures taken of 'Ayló'chaxnim on 2020 November 24. The asteroid can be seen moving past the barred spiral galaxy NGC 5584 in the southeast direction at \sim 120 arcseconds per hour in resulting in a \sim 6 arcsecond spacing between the two exposures separated by a 3 minute time interval. The cardinal directions and spatial scale are indicated for reference.

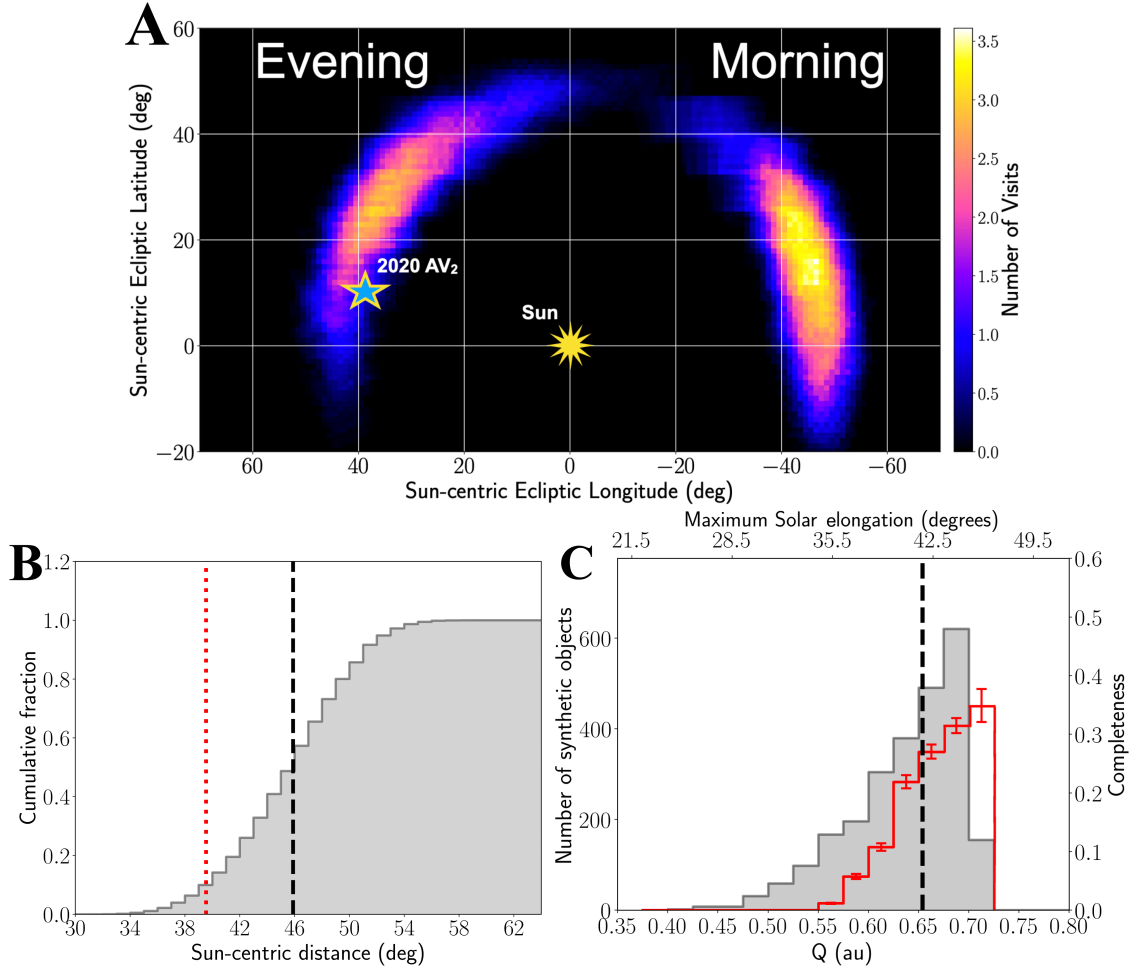


Figure 2: ZTF Twilight survey skyplane coverage. (A) Skyplane distribution of Twilight Survey coverage occurring between 2019 September 19 UTC and 2020 January 30 UTC. The star plots the discovery locations of inner-Venus asteroid 'Ayló'chaxnim. The color scale is the number of ZTF visits per square degree as a function of ecliptic longitude and latitude. (B) Cumulative distribution of the Sun-centric distance of the Twilight survey footprints between 2020 September 19 UTC and 2020 January 30 UTC. The vertical back dashed line shows the maximum possible Sun-centric distance of inner-Venus objects and the vertical red dotted line shows the Sun-centric distance of 'Ayló'chaxnim at its time of discovery on 2020 January 4 UTC. (C) Synthetic aphelion, Q , distribution and completeness of inner-Venus objects generated from the NEA model (6) and our survey completeness calculation. The 1- σ error bars on the completeness are determined assuming Poissonian statistics. The vertical dashed line shows the aphelion of 'Ayló'chaxnim. The second Y-axis shows the maximum solar elongation of the synthetic inner-Venus object population as a function of aphelion.

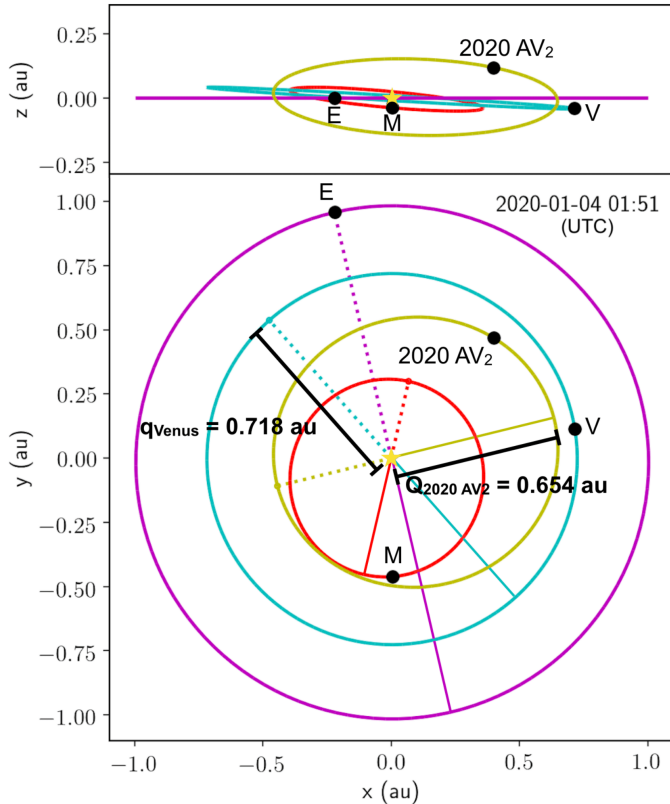


Figure 3: Orbital configuration of 'Ayló'chaxnim and the terrestrial planets at the time of its discovery. The orbit of Earth (purple), Venus (blue) and Mercury (red) and 'Ayló'chaxnim (green) on 2020 January 4 UTC looking from above the orbital plane of the inner Solar System. The orbit plotted for 'Ayló'chaxnim in this figure is taken from the orbital elements in Tab. S1. The perihelion directions of 'Ayló'chaxnim and the planets are plotted with dotted lines. The aphelion directions of 'Ayló'chaxnim and the planets are plotted with solid straight lines.

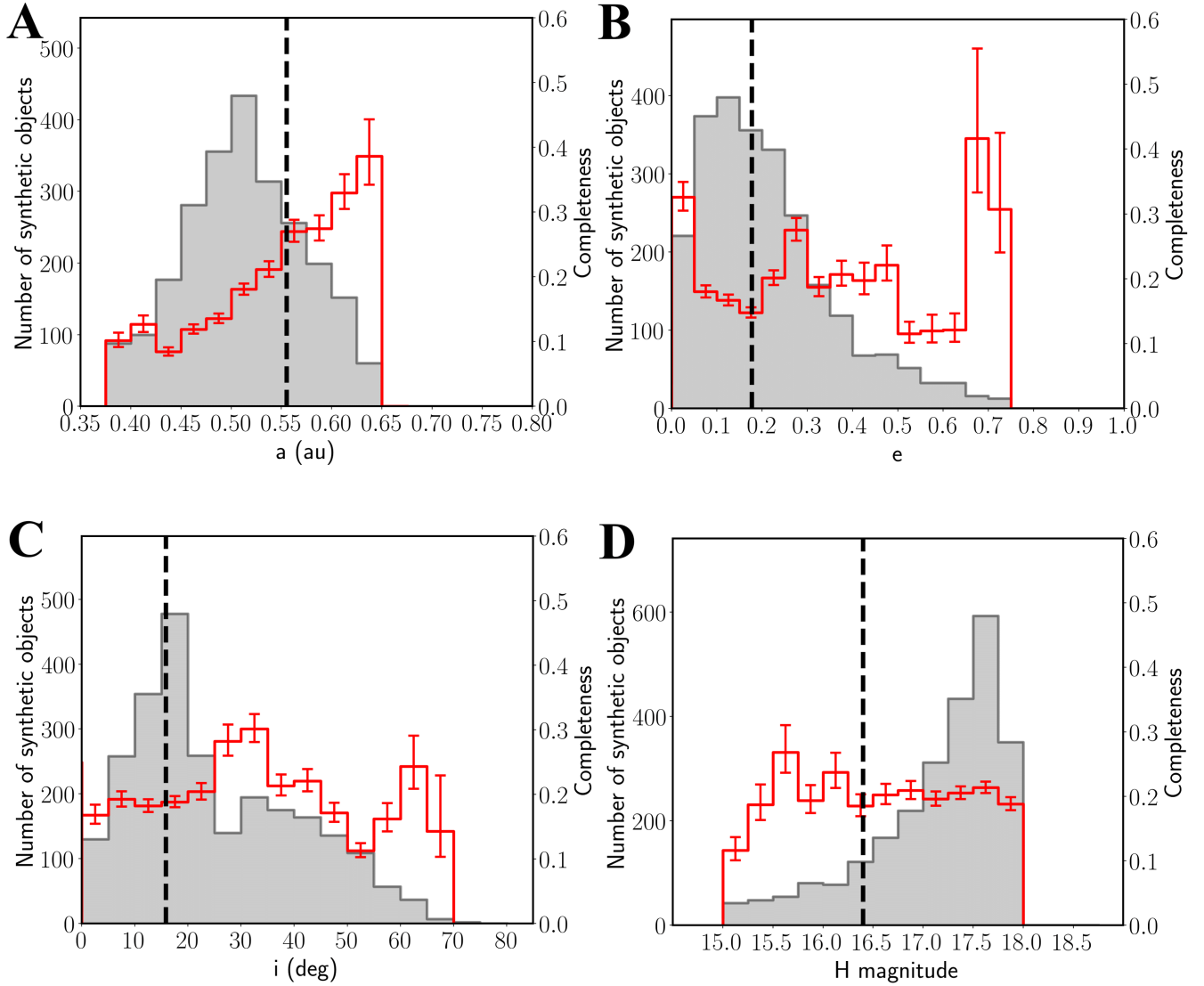


Figure 4: Orbital distribution and completeness of synthetic inner-Venus asteroids. Comparison between the (A) semi-major axis, a , (B) eccentricity, e , (C) inclination i and (D) absolute magnitude H distribution of the number of synthetic inner-Venus asteroids generated from the NEA model (6) (grey histograms) and the completeness of synthetic inner-Venus asteroids detected in the survey simulation (red histogram). The $1-\sigma$ error bars on the completeness are determined assuming Poissonian statistics. The vertical dashed black line indicates the value of the element for 'Ayló'chaxnim from Tab. S1. The absolute magnitude range of 15 to 18 corresponds to asteroids in the size range of $\sim 1\text{-}3$ km assuming a 20% surface reflectivity. The number of objects from the NEA model has been oversampled by a factor of 1,000.



Supplementary Materials for

A kilometer-scale asteroid inside Venus's orbit

B. T. Bolin*, W.-H. Ip, F. J. Masci, Q. Ye, E. A. Kramer, G. Helou, T. Ahumada, M. W. Coughlin, M. J. Graham, R. Walters, K. P. Deshmukh, C. Fremling, Z.-Y. Lin, J. W. Milburn, J. N. Purdum, R. Quimby, D. Bodewits, C.-K. Chang, C.-C. Ngeow, H. Tan, C. Zhai, P. van Dokkum, M. Granvik, Y. Harikane, L. A. Mowla, K. B. Burdge, E. C. Bellm, K. De, S. B. Cenko, C. M. Copperwheat, R. Dekany, D. A. Duev, D. Hale, M. M. Kasliwal, S. R. Kulkarni, T. Kupfer, A. Mahabal, P. J. Mróz, J. D. Neill, R. Riddle, H. Rodriguez, E. Serabyn, R. M. Smith, J. Sollerman, M. T. Soumagnac, J. Southworth, L. Yan

*correspondence to: bbolin@caltech.edu

This PDF includes:

Materials and Methods

Figs. S1 to S5

Table S1

Materials and Methods

Discovery, follow-up and orbital determination:

The initial discovery observations of (594913) 'Ayló'chaxnim on 2020 January 4 were made in four sidereally-tracked 30 s r-band exposures by the 48-inch Samuel Oschin Telescope. The observations were made during evening astronomical twilight while the telescope was pointing at 25.5 degrees elevation and the center of the telescope's field of view was pointing through 2.3 airmasses. The brightness of 'Ayló'chaxnim during its discovery observations were $r \sim 18.1$ magnitude and was moving approximately ~ 130 arcseconds per hour. The observations were taken during average seeing conditions for the Palomar site with nearby stellar objects of similar brightness to 'Ayló'chaxnim having FWHM ~ 2.1 arcseconds. The sky plane rate of motion of 'Ayló'chaxnim during the observations was 2.1 arcseconds/min resulting in no significant trailing losses of the individual detections of 'Ayló'chaxnim in the discovery images (Fig. 1, A-B). The mean airmass of the observations was ~ 2.3 .

The preliminary orbit of 'Ayló'chaxnim determined from the discovery observations was first classified as an Apollo-like orbit based on the initial discovery observations with $a \sim 1.53$ au and eccentricity $e \sim 0.45$ with a near-Earth asteroid (NEA) digest2 score of 98 (31). After including the SEDM and KPED observations made on 2020 January 8 and 9, the semi-major axis became $a \sim 0.551$ au ± 0.004 , eccentricity $e \sim 0.191 \pm 0.008$ resulting in an aphelion $Q \sim 0.657 \pm 0.001$ au. Additional observations taken by other groups up until January 23 later revised to $Q = 0.654 \pm 0.001$, a $>50\sigma$ confidence interval smaller than the 0.72 au perihelion distance of Venus. Additional recovery observations were obtained by SEDM and the Lulin Optical Telescope on November 24-26 which expanded the orbital arc by an order of magnitude to 327 days greatly improving the orbit where $Q = 0.653738 \pm 9.53 \times 10^{-7}$ (Supplementary Material Tab. S1 and Fig. S2). The effect of airmass on the size of astrometric uncertainties of observations at the Palomar Observatory site are small, increasing to $<0.08\text{-}0.10$ arcseconds at

the 2.0-3.0 airmass range of the observations of 'Ayló'chaxnim (12). No pre-discovery observations of 'Ayló'chaxnim were located in the ZTF archive.

Twilight Survey strategy:

Previous searches for asteroids within the orbit of Earth and of Venus have included the use of small-field CCD cameras on ground-based meter-scale telescopes to image portions of the sky within 90-degrees Solar elongation (32). Previous attempts to search for objects interior to the orbit of the Earth and of Venus with wide-field CCD imagers have been made by the European Near Earth Asteroids Research (EURONEAR) project based on the 2.5 m Isaac Newton Telescope at the Roque de los Muchachos Observatory (ORM) on La Palma, Canary Islands, Spain (33) and by ZTF (14).

The strategy of our search for interior to Earth and interior to Venus objects is a modified strategy with ZTF is modified compared to previous searches with ZTF (14). Astronomical twilight time is used by ZTF to search for Solar System objects at small Solar elongations <60 degrees from the Sun in a program called the “Twilight Survey” during which 'Ayló'chaxnim was discovered. Searching for Solar System objects so close to the Sun during twilight is accomplished by using the 47 sq. degree field of view and minimum elevation of the 48-inch Samuel Oschin Telescope to point the telescope as close to the horizon as possible during evening and morning Astronomical twilight when the Sun is \sim 18 degrees below the horizon (11). This results in being able to search the night sky to as close as \sim 35 degrees from the Sun, corresponding to potentially detecting objects as close as \sim 0.57 au from the Sun. Twilight observing sessions are conducted each night, alternating between evening and morning twilight on sequential nights.

Discovery, follow-up and characterization observations:

Zwicky Transient Facility, ZTF: The ZTF camera consists of 16 separate 6144 x 6160-pixel arrays on a single CCD camera mounted on the 48-inch Samuel Oschin Telescope at Palomar

Observatory and is robotically operated. The plate scale of the camera is 1.01 arcseconds/pixel and has a 7.4-degree x 7.4-degree field of view (8, 34). The data processing pipeline produced images differenced from reference frames and removes or masks most detector artifacts. Transients are extracted from the images and several algorithms are used to identify slower moving objects that appear as round PSF detections in the images (12) and to extract fast-moving objects that appear as streaked detections (13, 35). Moving objects can be identified in images taken in each of its *g*, *r* and *i* band filters. For the purpose of the Twilight Survey, 30 s exposures were used with the *r* filter. Seeing was measured to be \sim 2.1 arcsec from stars near the detection of 'Ayló'chaxnim in the discovery images.

Spectral Energy Distribution Machine, SEDM: Observations taken by the SEDM used the Rainbow Camera consisting of two identical Princeton Instruments Pixis 2048B eXelon model 2048 x 2048 pixel CCDs mounted on the Palomar 60-inch telescope and is robotically operated (15, 36). The Rainbow Camera has a 13 arcminute x 13 arcminute field of view divided into four \sim 6 arcminute quadrants with each having coverage of a single filter, *u*, *g*, *r* and *i* and a 0.37 arcseconds/pixel spatial scale. Only the *r* filter quadrant was used for our follow-up observations with SEDM with non-sidereally tracked 30 s exposures. Seeing conditions were \sim 1.75 arcsec as measured for background stars in the follow-up images. For the 2020 November 24 recover observations of 'Ayló'chaxnim, 120 s exposure in *r* band were used and the seeing conditions were \sim 1.5 arcseconds and the airmass was \sim 3.3.

Kitt Peak Electron Multiplying CCD Demonstrator, KPED: The KPED instrument is mounted on the Kitt Peak 84-inch telescope and consists of a 1024 x 1024 pixel Electron Multiplying CCD camera and is robotically operated (16). The camera has a spatial scale of 0.26 arcseconds/pixel and a 4.4 arcminute x 4.4 arcminute field of view. The camera is capable of reading out at a rate of 1 Hz and of individual exposures times up to 10 s. Our observations used 10 s exposures in *r*-band and were sidereally tracked due to the short exposure time. Seeing condi-

tions were ~ 1 arcsec as measured for background stars in the follow-up images.

Keck I Telescope: The Low Resolution Imaging Spectrometer (LRIS) (37) on the Keck I telescope was used to observe 'Ayló'chaxnim on 2020 January 23 in spectroscopy mode (Program ID C272, PI M. Graham). Both the blue camera consisting of a $2 \times 2K \times 4K$ Marconi CCD array and the red camera consisting of a science grade Lawrence Berkeley National Laboratory $2K \times 4K$ CCD array were used. Both cameras have a spatial resolution of 0.135 arcsec/pixel. The 1.0-arcsecond wide slit was used with the 560 nm dichroic with $\sim 50\%$ transmission efficiency in combination with the 600/4000 grating for the blue camera and the 400/8500 grating for the red camera providing a spectral resolution of 0.4 nm and 0.7 nm, respectively (37, 38). A total exposure time of 600 s over two integrations were taken in seeing conditions of ~ 0.6 arcseconds measured at zenith, however, the observations were taken at the large airmass of ~ 3.4 significantly degrading the seeing to ~ 1.2 arcsec. Wavelength calibration was completed using the HgCdZn lamps for the blue camera and the ArNeXe lamps for the red camera. Flux calibration was completed with the G191-B2B and Feige 34 standard stars for the blue and red camera respectively and a Solar analog 2MASS 22462446+0029244 was used to produce the reflectance spectrum as seen in (Fig. 3).

Lulin Optical Telescope: The 1 m Lulin Optical Telescope (LOT) using the $2K \times 2K$ SOPHIA camera (39) at Lulin Observatory was used to provide recovery data of 'Ayló'chaxnim on 2020 November 25-26. Data were taken in Johnson-Cousins *R* filter, and the telescope was tracked non-sidereally at the asteroid's sky motion rate and 120 s exposures were used. The seeing during the observations was ~ 2 arcseconds and the airmass of the observations was ~ 2.8 .

Visual imaging/spectroscopy reduction and astrometry: All visual imaging data was reduced using custom code for bias and flat field detrending. The LRIS spectroscopic data were reduced using flat field, dark current and arc lamp exposures with the LPipe spectroscopy reduction software (40). The *Gaia* data release 2 catalog (41, 42) was used with the ZTF data

reduction pipeline (12) to produce an astrometric solution on ZTF data and with the Astrometrika software (43). Photometric calibration was performed using the Pan-STARRS1 catalog database (44).

Dynamical integration: We used the `rebound` N-body orbit integration package (45) using the `IAS15` adaptive time step integrator (46) to determine the orbital history of 'Ayló'chaxnim. Using the multi-variate distribution of the orbital parameters presented in Tab. S1 and Fig. S2 based on the orbit of 'Ayló'chaxnim determined by using our discovery and follow-up observations spanning 327 days between 2020 January 4 to 2020 November 26 and the `Find_Orb` orbital integration package, we generated several hundred clone orbits of 'Ayló'chaxnim. We integrated the 'Ayló'chaxnim orbitak clones forwards and backward 30 Myrs using barycentric coordinates with a nominal timestep of 14 h. Because it is an adaptive time-step integrator, `IAS15` will decrease the time of this time step during close encounters to avoid discrepancies in the orbits of test particles resulting from too coarse time steps. We find that 'Ayló'chaxnim has experienced numerous, ~ 0.01 au close encounters with Mercury and Venus that are as frequent as every few hundred to thousands of years. The effect of perturbations during planetary encounters on the orbital evolution of planet-cross asteroids in the terrestrial planet zone has been shown to eclipse the Yarkovsky effect on the time scales of our orbital integrations (6, 47, 48), therefore, we neglect the Yarkovsky effect in our orbital integrations of the clones of 'Ayló'chaxnim.

Comparison with the NEA population and size estimate: One of the dynamical pathways for inner-Venus asteroids is to originate from the Main Asteroid belt through source regions located near various major planetary resonances (49). If we assume that 'Ayló'chaxnim originated from the Main Belt as an asteroid family fragment (50) before crossing inside of the orbit of Venus, asteroids with orbits similar to 'Ayló'chaxnim according to the Granvik et al. (2018) NEA model most likely originate with a $\sim 77\%$ probability from the ν_6 resonance that forms the boundary

of the inner Main Belt at 2.2 au (51). The second most likely source of 'Ayló'chaxnim with a $\sim 18\%$ probability are the Hungaria asteroid population located just exterior to the Main Belt at 2.0 au (52) and the third most likely at $\sim 4\%$ being the 3:1 mean motion resonance with Jupiter located in the Main Belt at 2.5 au (53).

The the main contributor to the uncertainty on the $\sim 1.6 \pm 0.6$ km diameter estimate of 'Ayló'chaxnim is made using a $1-\sigma$ uncertainty on H of ~ 0.8 magnitudes from the JPL Small-Body Database Browser. We note that the ~ 0.8 magnitude estimate on H is greater than the ~ 0.3 magnitudes scatter on H of asteroids from the Minor Planet Center catalog (54), which seems reasonable considering uncertainty caused by the unknown phase function of 'Ayló'chaxnim and the large $\sim 100^\circ$ phase angle the asteroid was observed at in 2020 January (55). We obtain a slightly lower diameter for 'Ayló'chaxnim of ~ 1.3 - 1.5 km using albedos (in the range 0.23-0.3) measured for S-types in the general NEA population (56). Combining the spread in albedos of S-type asteroids from (56) to our estimate of the albedo of 'Ayló'chaxnim and the ~ 0.8 magnitudes uncertainty on H , we estimate a diameter range for 'Ayló'chaxnim of ~ 1 - 2 km.

The number of asteroids the NEA model predicts in the H range $15 < H < 18$ is $\sim 1,150$ asteroids. In $15 < H < 18$, $\sim 0.2\%$ or ~ 2 are inner-Venus asteroids (6). The number of inner-Venus asteroids predicted by the NEA model shrinks to 0.3 ± 0.6 when we consider only asteroids brighter than the nominal H for 'Ayló'chaxnim of $\sim 16.4 \pm 0.8$. The absolute magnitude of 'Ayló'chaxnim was made using an assumption for the phase parameter of 0.15. The value of 0.15 is the average asteroid phase parameter as determined by photometric observations of a large ensemble of asteroids regardless of spectral class (54, 57). The spectral type of 'Ayló'chaxnim has been constrained to have a likely S-type taxonomy from ours and other's spectral observations of it. Therefore, it might be appropriate to assume a higher phase parameter of ~ 0.2 found for S-types (54, 58) which would increase the nominal absolute magnitude of

'Ayló'chaxnim by ~ 0.1 magnitudes, tiny compared to our uncertainties on the absolute magnitude value for 'Ayló'chaxnim of ~ 0.8 magnitudes. Assuming a slightly ~ 0.1 magnitude larger nominal absolute magnitude of 'Ayló'chaxnim would only slightly increase the expected number of inner-Venus asteroids predicted by the NEA model by < 0.1 . We also note that the scatter in phase parameters determined for asteroids within the S-types taxonomic class is ~ 0.1 - 0.2 when measured over a large ensemble of asteroids (54, 59), and thus the nominal value for the phase parameter of ~ 0.2 for S-type asteroids is compatible with our assumed phase parameter value of 0.15 used to obtain an absolute magnitude value of 16.4 for 'Ayló'chaxnim.

Estimating the ZTF inner-Venus asteroid population completeness: Synthetic observations of IVOs were generated using a survey simulator (60) and the IVO population described by the NEA model as input test particles into the simulation (6). The synthetic IVO population was oversampled from the NEA model by a factor of 1,000 using a medium resolution version of the NEA model with $da = 0.05$ au, $de = 0.02$, $di = 2.0^\circ$, $dH = 0.25$. We used synthetic IVOs with $15 < H < 18$ because this fully covers the absolute magnitude value of 'Ayló'chaxnim. We refined our synthetic inner-Venus asteroid observations by calculating the efficiency for each synthetic inner-Venus asteroid detection in each field. The per object per field efficiency is estimated by comparing actual detections of known moving objects serendipitously observed in the Twilight Survey fields with the predicted number of known objects detected in the fields. The Twilight Survey per object efficiency as a function of V magnitude is presented in Fig. S5 (C). A function of the form

$$\epsilon(V) = \epsilon_0 \left[1 + \exp \left(\frac{V - V_{lim}}{V_{width}} \right) \right]^{-1} \quad (1)$$

is used to interpolate the per-field efficiency with $\epsilon_0 = 0.87$ representing the maximum possible efficiency for detecting moving objects, $V_{lim} = 20.60$ mag, representing the limiting magnitude of the survey where the efficiency drops to half for detecting moving objects and $V_{width} = 0.74$ representing the width of the transition in the drop of the efficiency in detection faint moving

objects (55) and is plotted as a red line in Fig. S5 (C). We note that the value of $\epsilon_0 = 0.87$ is remarkably close to the fill factor of ZTF (8) suggesting that the limiting factor in detecting bright moving objects by ZTF is the detector layout rather than the ZTF processing pipeline (12). An $\epsilon(V) = 0.87$ is assumed for bright object detections with $V > 17.5$. The Twilight Survey per object per field efficiency in Fig. S5 (C) is determined by averaging the efficiency calculated over the pointings in the Twilight survey between 2019 September and 2020 January. A histogram of the exposure-based limiting magnitudes of fields taken during the Twilight survey between 2019 September and 2020 January is presented in Fig. S5 (D). The limiting magnitudes in Fig. S5 (D) are the 5σ limiting values in the Twilight survey pointing with no assumption or correction regarding the efficiency of asteroid detections. Therefore, the raw 5σ limiting exposure-based survey magnitudes may actually correspond to higher efficiency levels on average.

In addition to the limiting magnitude, trailing losses due to the sky plane motion of the inner-Venus asteroids could further decrease the efficiency calculated with Eq. (1) (55). However, as seen in Fig. S5 (B), the vast majority of synthetic inner-Venus asteroid detections have a sky plane rate of motion of 240 arcseconds per hour or slower which does not result in significant trailing of the detections given the typical 2 arcseconds seeing at the Palomar observing site. The lack of preference for slower-moving objects seen in the rate of motion distribution of the detected number of objects plotted in red in Fig. S5 (B) compared to the rate of motion distribution of synthetic inner-Venus asteroids suggests that losses due to trailing within the inner-Venus asteroid population are negligible.

The per inner-Venus asteroid, j , per session, n , efficiency, $\epsilon_{j,n}(V_{j,n})$ is given by its per session field visible magnitude, $V_{j,n}$ using equation Eq. (1). If a synthetic inner-Venus asteroid is not seen >3 times or not seen at all during a given session n , $\epsilon_{j,n}(V_{j,n}) = 0$. The vast majority of synthetic inner-Venus asteroids have V magnitude < 20 as seen in Fig. S5 (A) resulting in the majority of inner-Venus asteroid detections located in Twilight Survey fields having

$$\epsilon_{j,n}(V_{j,n}) > 70\%.$$

The probability of detecting a single Synthetic inner-Venus asteroid, j , p_j , over the total n_{max} Twilight Survey sessions is given by the following equation

$$p_j = 1 - \prod_{n=0}^{n_{max}} [1 - \epsilon_{j,n}(V_{j,n})] \quad (2)$$

where $n_{max} = 89$ corresponding to 90 individual Twilight Survey sessions. The number of detected synthetic inner-Venus asteroids is weighted per synthetic inner-Venus asteroid a , e , i and H bin by each detected object's p_j . The completeness of synthetic inner-Venus asteroids detected by the synthetic ZTF survey per synthetic inner-Venus asteroid a , e , i and H bin is calculated by dividing the weighted number of synthetic inner-Venus asteroids detected per synthetic inner-Venus asteroid a , e , i and H bin by the total number of synthetic inner-Venus asteroids generated from the NEA model per synthetic inner-Venus asteroid a , e , i and H bin. The completeness of inner-Venus asteroids detected per a , e , i and H bin is plotted with a red line in Fig. 4 (A-D). Marginalizing over the complete a , e , i and H distribution of the synthetic inner-Venus asteroid population results in an integrated completeness of ~ 0.15 and a completeness of ~ 0.18 when considering inner-Venus asteroids within a 68.2% confidence interval encompassing 'Ayló'chaxnim's H magnitude. We repeated the completeness calculation use a variety of slope parameters representative of the different Q, S, C, D and X taxonomic types (54, 58) and found that the different slope parameter values did not significantly alter the completeness result. As discussed above, assuming a slightly larger phase parameter for 'Ayló'chaxnim to estimate its absolute magnitude only slightly increases the number of inner-Venus asteroids predicted by the NEA model and thus will only increase the expected number of inner-Venus objects detected in the twilight survey by $\sim 1\%$.

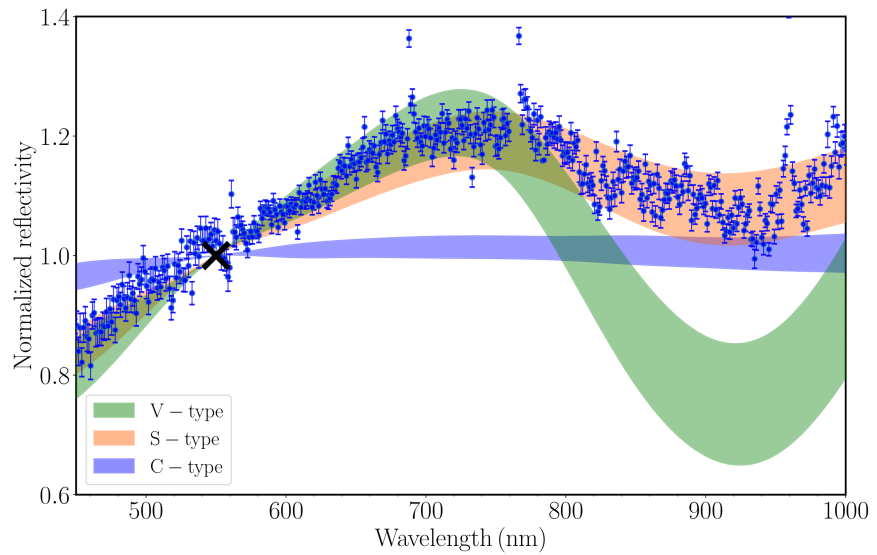


Figure S1: Visible wavelength reflectance spectrum taken of 'Ayló'chaxnim. Taken with the LRIS instrument on Keck I on 2020 January 23, the spectrum of 'Ayló'chaxnim is plotted as blue dots. The error bars on the spectrum data points correspond to $1-\sigma$ uncertainty. The spectrum has been normalized to unity at 550 nm indicated by the black cross. The spectrum presented was obtained by combining two spectra from the blue camera using the 600/4000 grating and the red camera using the 400/8500 grating with a 560 nm dichroic (37, 38). The data have been rebinned and smoothed by a factor of 10 using an error-weighted mean. The dip in the spectrum at ~ 560 nm is due an artifact caused by the dichroic solution and the spikes at ~ 770 nm and ~ 960 nm are caused by the telluric H_2O absorption features in both the asteroid and Solar analog spectra. The spectral range of S, V and C-type asteroids from the Bus-DeMeo asteroid taxonomic catalogue (61) are over-plotted with the S-type spectrum most closely resembling the spectra of 'Ayló'chaxnim.

Table S1: **Orbital elements of 2020 AV₂.** Based on observations collected between 2020 January 4 UTC to 2020 November 26 UTC. The orbital elements are shown for the Julian date (JD) shown using the software `Find_Orb` by Bill Gray. The $1-\sigma$ uncertainties are given in parentheses. The value and $1-\sigma$ uncertainties for H is provided by the JPL Small-Body Database Browser entry for 'Ayló'chaxnim.

Element	
Epoch (JD)	2,459,179.5
Time of perihelion, T_p (JD)	2,458,907.045±(0.019)
Semi-major axis, a (au)	0.555443170±(3.65x10 ⁻⁷)
Eccentricity, e	0.17696610±(2.33x10 ⁻⁶)
Perihelion, q (au)	0.45714852±(1.56x10 ⁻⁶)
Aphelion, Q (au)	0.653737830±(9.53x10 ⁻⁷)
Inclination, i (°)	15.86824±(0.00014)
Ascending node, Ω (°)	6.70827±(0.00035)
Argument of perihelion, ω (°)	187.32773±(0.00053)
Mean Anomaly, M (°)	288.6292±(0.0011)
Absolute Magnitude, H	16.4±(0.8)

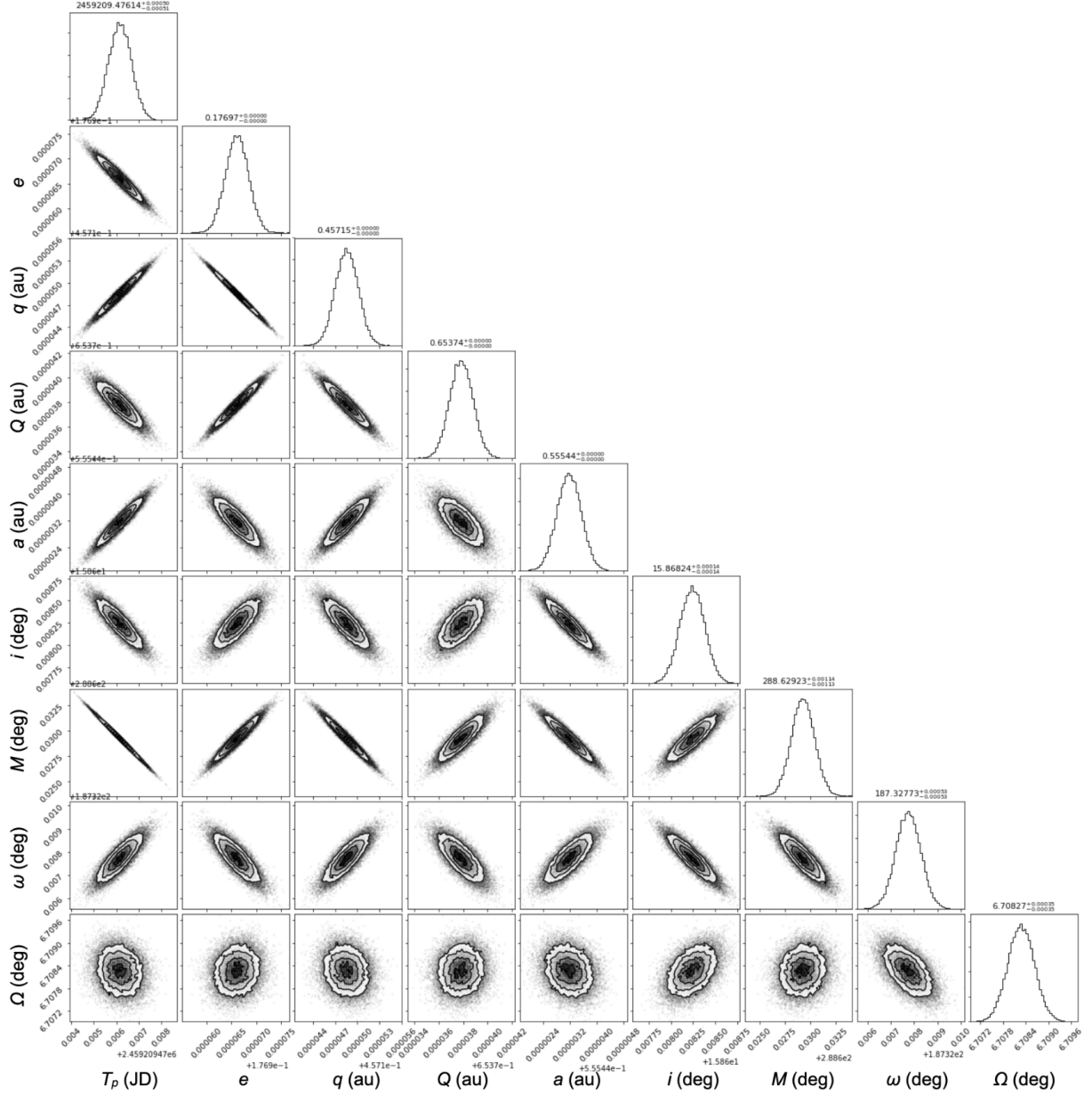


Figure S2: Distribution of 'Ayló'chaxnim orbital element samples. Corner plot of 30,000 samples from the multivariate distribution of orbital elements of 'Ayló'chaxnim from the covariance obtained with the orbit fit from observations between 2020 January 4 UTC to 2020 November 26 UTC. The central value and the $1-\sigma$ uncertainty for each parameter value is given at the top of each column in the corner plot.

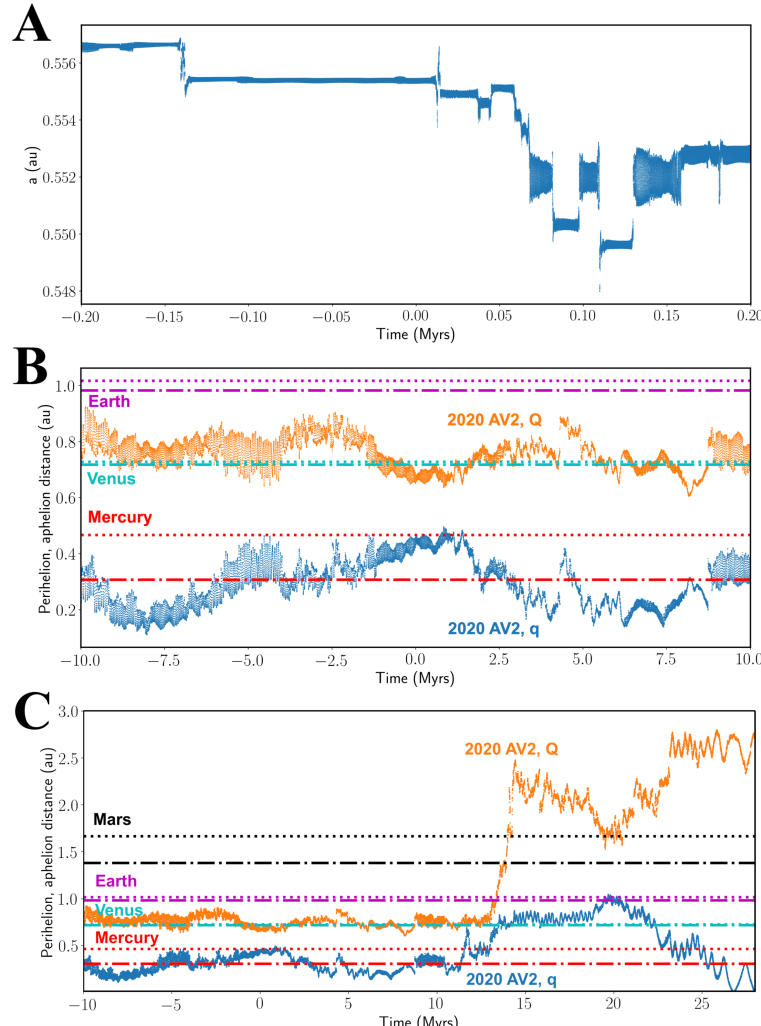


Figure S3: Time evolution of one of the possible orbital histories of 'Ayló'chaxnim based on the orbital clones representing its orbit from Tab. S1. (A) Possible time evolution of the semi-major axis of 'Ayló'chaxnim represented by its nominal orbit in Tab. S1. The plateaus in the evolution of the semi-major axis separated by jumps are due to 'Ayló'chaxnim crossing resonances with Venus and Jupiter. At around 0.06 Myrs, 'Ayló'chaxnim entered a 3:2 mean motion resonance with Venus located at 0.552 au that lasts for a 0.01 Myrs before jumping in out of the resonance for the next \sim 0.1 Myrs. (B) The evolution of the aphelion (orange) and perihelion (blue) distances of an orbital clone of 'Ayló'chaxnim representing the nominal orbit integrated to \pm 10 Myrs. The current aphelion (dashed line) and perihelion distances (dash-dot line) are plotted as horizontal lines for Mercury (red), Venus (cyan) and Earth (purple). The aphelion distance of 'Ayló'chaxnim spends only \sim 2 Myrs of the simulation within the perihelion distance of Venus (0.718 au) and the perihelion distance less than the aphelion distance of Mercury (0.467 au) for most of the simulation and crosses Mercury's perihelion distance (0.307 au) at \sim 2 Myrs having a minimum perihelion of \sim 0.1 au. (C) Time evolution of a particularly long-lived clone integrating its orbital evolution to 28 Myrs. The aphelion (dashed line) and perihelion distances (dash-dot line) are plotted as horizontal lines for Mercury (red), Venus (cyan), Earth (purple) and Mars (black). A close encounter with the Venus of \sim 0.01 au at \sim 13 Myrs and subsequent perturbations from the other planets results in 'Ayló'chaxnim eventually increasing in its aphelion distance and decreasing its perihelion distance until it collides with the Sun with a perihelion distance of <0.005 au at \sim 28 Myrs.

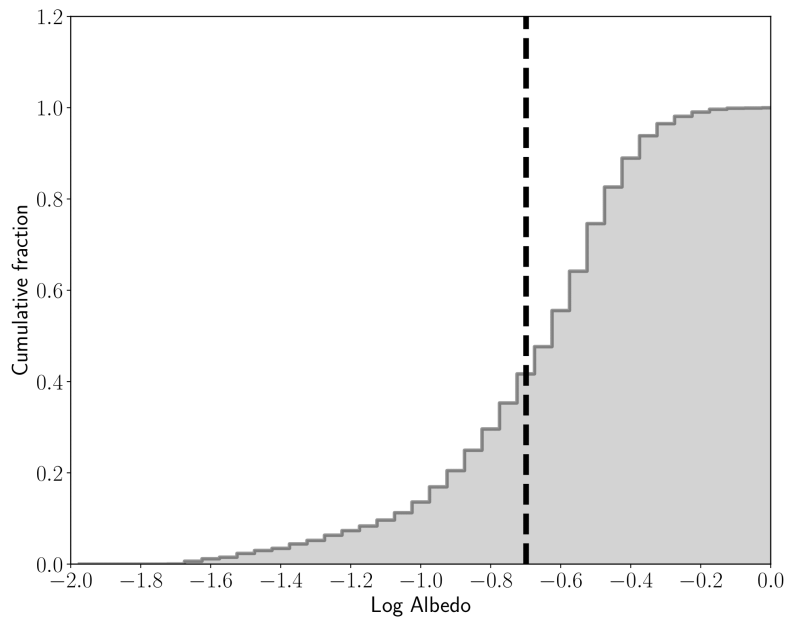


Figure S4: Albedo cumulative distribution of inner-Venus objects. The cumulative distribution of inner Venus objects with $15 < H < 18$ adapted from the NEA albedo model (24). The predicted albedo of 'Ayló'chaxnim is indicated by the location of the dashed vertical line.

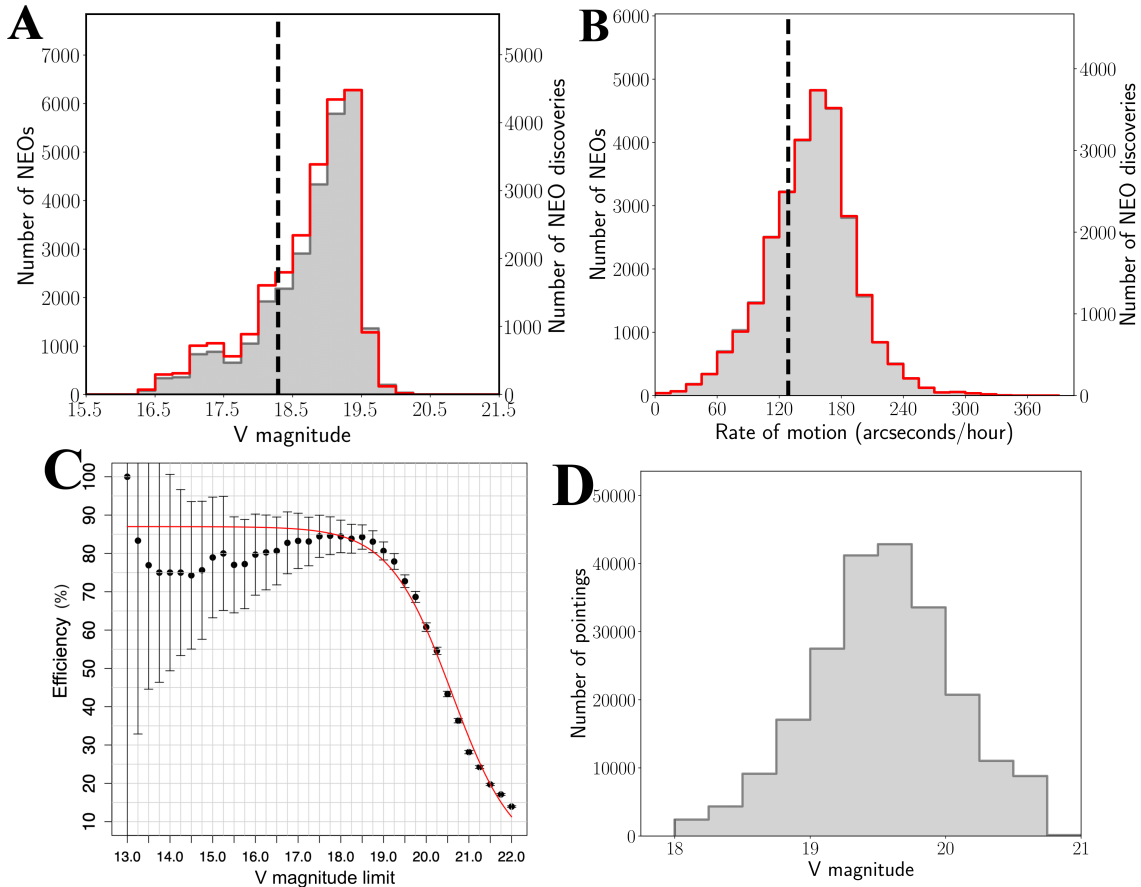


Figure S5: Synthetic inner-Venus asteroid V magnitude and rate of motion distributions and detection efficiency. (A) Comparison of the synthetic inner-Venus asteroid apparent V magnitude distribution (grey histogram) with the efficiency weighted V magnitude distribution of detected inner-Venus asteroids in the survey simulation (red histogram). Detections are weighted using Eqs. (1) and (2). (B) Same as (A), but for the synthetic inner-Venus asteroid's rate of motion. The vertical dashed lines in (A) and (B) are the values of the apparent V magnitude and rate of motion of 'Ayló'chaxnim on 2020 January 4 UTC. (C) Detection efficiency of asteroids in the Twilight survey as a function of V magnitude. The 1- σ error bars are determined assuming Poissonian statistics. Eq. (1) using $\epsilon_0 = 0.87$, $V_{lim} = 20.60$, $V_{width} = 0.74$ is plotted in red. (D) The exposure-based 5- σ limiting magnitude of the Twilight survey pointings between 2019 September 20 UTC and 2020 January 30 UTC with no assumptions or corrections regarding the efficiency of the detections in the pointings.